

Supporting information

One-step coating commercial Ni nanoparticles with Ni, N-codoped carbon shell towards efficient electrocatalysts for CO₂ reduction

Fangxin Mao, Peng Fei Liu, Pengfei Yang, Jinlou Gu* and Hua Gui Yang*

AUTHOR INFORMATION

Corresponding Authors

*Hua Gui Yang: hgyang@ecust.edu.cn

*Jinlou Gu: jinlougu@ecust.edu.cn

Experimental section

Chemicals and reagents. Ni nanopowder (50 nm, 99.9% trace metals basis) was purchased from Aladdin. Urea (H₂NCONH₂, 99%), potassium thiocyanate (KSCN, 99%) and potassium hydrogen carbonate (KHCO₃, >99.5%) were purchased from Sinopharm Chemical Reagent Co. Ltd, Nickel phthalocyanine (NiPc, 95%) and nano nickel oxide (NiO, 99.9%) were purchased from J&K Scientific Ltd. The deuterium oxide (D₂O) containing 0.05wt.% 3-(trimethylsilyl)propionic-2,2,3,3-d₄ acid (TMSP), sodium salt, was purchased from Sigma-Aldrich. High purity argon (Ar), nitrogen (N₂) and carbon dioxide (CO₂) gases were provided by the Shanghai Jiajie Special Gas Co., Ltd. All the aqueous solutions were prepared with deionized water (>18.25 MΩ cm) produced by the Millipore system and the chemicals were used without further

purification.

Synthesis. Ni NPs@NiNC-20 was prepared by developed solid powder pyrolysis method. Typically, 150 mg commercial Ni nanopowder was grinded with 3000 mg urea powder ($m_{\text{urea}}/m_{\text{Ni}} = 20$) in an agate mortar for several minutes. The mixture was then transferred into a rectangular alumina ceramics crucible before annealing at 600 °C for 3 h, under N₂ flow with rate of 80 sccm. The products were collected for characterizations and electrochemical performance measurements after naturally cooling to the room temperature. Ni NPs@NiNC-4 and Ni NPs@NiNC-10 were prepared by the same procedure except for changing the ratio of $m_{\text{urea}}/m_{\text{Ni}}$ as 4 and 10, respectively.

Characterizations. The field-emission scanning microscope (FE-SEM, Hitachi S-4800) was used to capture the morphology images, operating at 15 kV for all the images. All the transmission electron microscopy (TEM) characterization was carried out on the JEM-2100F 200 keV S/TEM, and elements mapping images were captured with energy dispersive X-ray (TEM-EDX) detector. X-ray photoelectron spectroscopy (XPS) was measured on the Thermo ESCALAB 250 Xi with Al K α ($h\nu = 1486.6$ eV) monochromator, and the spectra were calibrated based on the binding energy of C1s. X-ray diffraction (XRD) patterns were acquired with Bruker D8 equipped with Cu K α 1 radiation (40 kV, 40 mA) under a scan rate of 5° min⁻¹ over the range of 10-80 ° (2θ). X-ray absorption fine structure spectroscopy (XAFS) were collected on the 1W1B beamline of the Beijing Synchrotron Radiation Facility (BSRF), China, and operated at ~200 mA and ~2.5 GeV under ambient temperature. The nuclear magnetic resonance

(NMR) spectrometer of Ascend 600 was used to collect the ^1H NMR spectra.

Electrode preparation. Glassy carbon electrode with diameter of 3 mm was applied as working electrode, on which the testing catalyst sample ink was dispensed. The ink solution was prepared by ultrasonic dispersion of the mixture containing 10 mg catalysts, 100 μL Nafion solution (5%), and 1.0 mL ethanol for 30 min. Then, 10 μL catalyst-containing ink was dropped onto the glassy carbon electrode by several times. The electrode was dried naturally under room circumstance before electrochemical test.

Electrochemical measurements. All electrochemical experiments were performed on the CHI-660e electrochemical station under ambient temperature. A hermetic two-compartment jacketed cell was assembled with a Nafion® proton-exchange membrane separating the counter electrode (platinum gauze) and the working electrode, that constitutes a standard 3-electrode system with a reference electrode (Ag/AgCl, 3.5 M KCl solution). The electrolyte is CO_2 -saturated 0.5 M KHCO_3 ($\text{pH}\approx 7.3$) aqueous solution for CO_2 reduction test. The reversible hydrogen electrode (RHE) potentials have been unitized based on the equation: $E_{\text{RHE}} = E_{\text{Ag/AgCl}} + 0.2046 + 0.0592 \times \text{pH}$. The electrochemically active surface area (ECSA) was estimated through electrochemical double-layer capacitance (C_{dl}). Cyclic voltammetry was implemented at different scan rates (50, 100, 300, 400, 500, and 750 mV s^{-1}) in a non-Faradaic region from +0.06 to +0.26 V vs. RHE in the CO_2 -saturated 0.5 M KHCO_3 . The C_{dl} was determined by plotting the $1/2 | j_{\text{a}} - j_{\text{c}} |$ at +0.16 V, in which the j_{a} and j_{c} are the anodic and cathodic current density, respectively. The slope means double-layer capacitance C_{dl} and the

ECSA can be evaluated from the electrochemical double-layer capacitance (C_{dl}) (ECSA = C_{dl}/C_{dlref} , where C_{dlref} is the specific capacitance of electrode with flat surface).

Products analysis. The gas products were quantified by online gas chromatography (GC), equipped the thermal conductivity detector (TCD for H_2) and a flame ionization detector (FID for CO and other gaseous hydrocarbons). The liquid products were measured by the 1H NMR with the internal standard of TMSP. For NMR measurement, 500 μL electrolyte was mixed with 100 μL D_2O containing TMSP.

The CO_2 gas flux was continuously pumped into the reaction cell at rate of 20 sccm controlled with the mass flow controller (Alicat Scientific, USA). The Faradaic efficiencies (FE) of the products (CO and H_2) were calculated as the formulas:

$$FE_{CO/H_2} = \frac{2x_{CO/H_2}pGF}{IRT}$$

The x (vol%) - the volume fraction of the target product in the gas flow. I is the total current at the specific applied potential. p (gas pressure) = 1.013×10^5 Pa, G (flow rate) = 20 mL min^{-1} , F (Faradaic constant) = 96485 C mol^{-1} , R (molar gas constant) = $8.314 \text{ J mol}^{-1} \text{ K}^{-1}$, T (temperature) = 298.15 K .

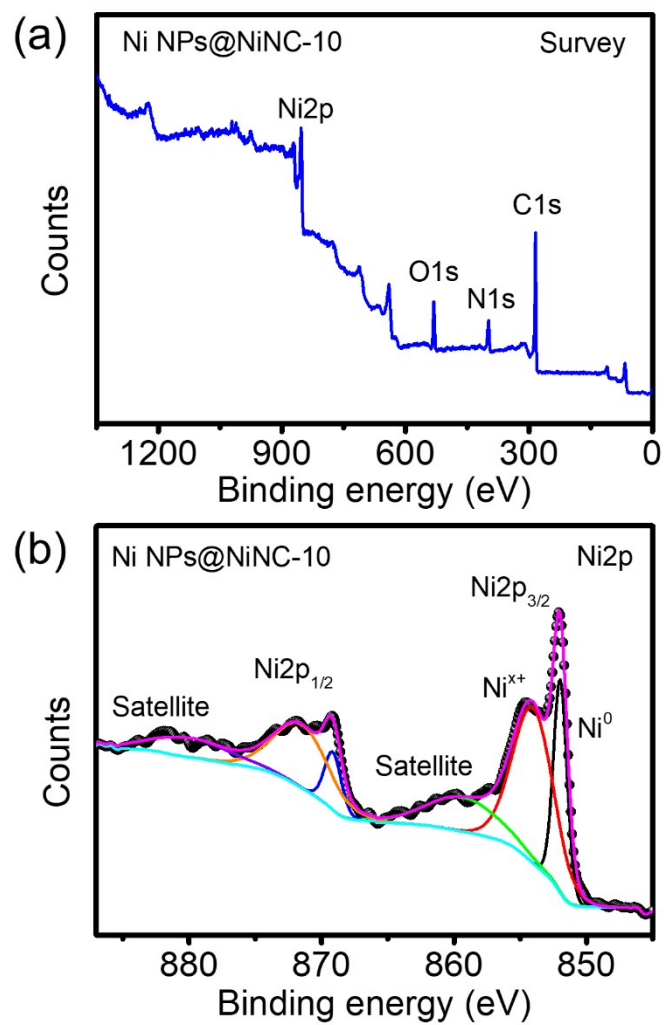


Fig. S1 (a) Survey and (b) Ni2p XPS spectra for Ni NPs@NiNC-10.

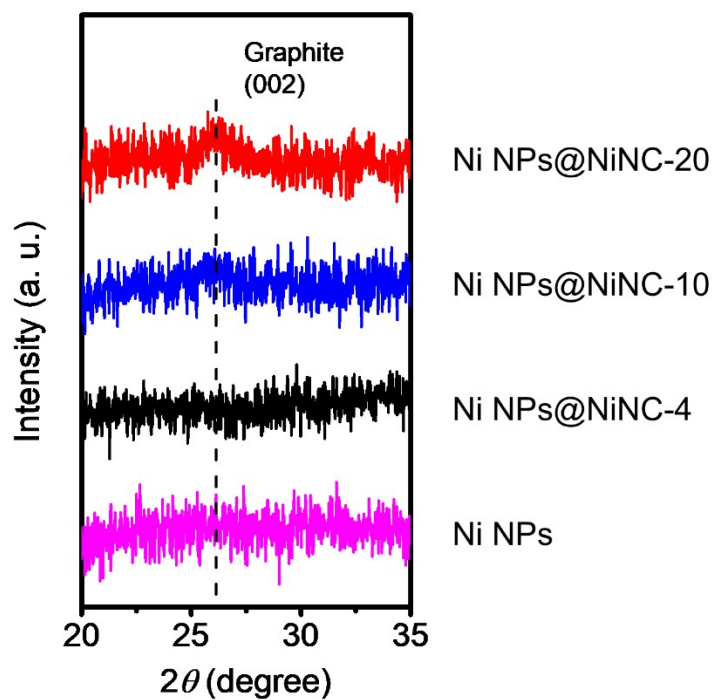


Fig. S2 Local magnified XRD patterns of Fig. 3a. A slight graphite (002) characteristic peak at 26.2° emerges on the pattern of Ni NPs@NiNC-20, indicating that high $m_{\text{urea}}/m_{\text{Ni}}$ ratio would be beneficial to the graphitization of carbon shell.

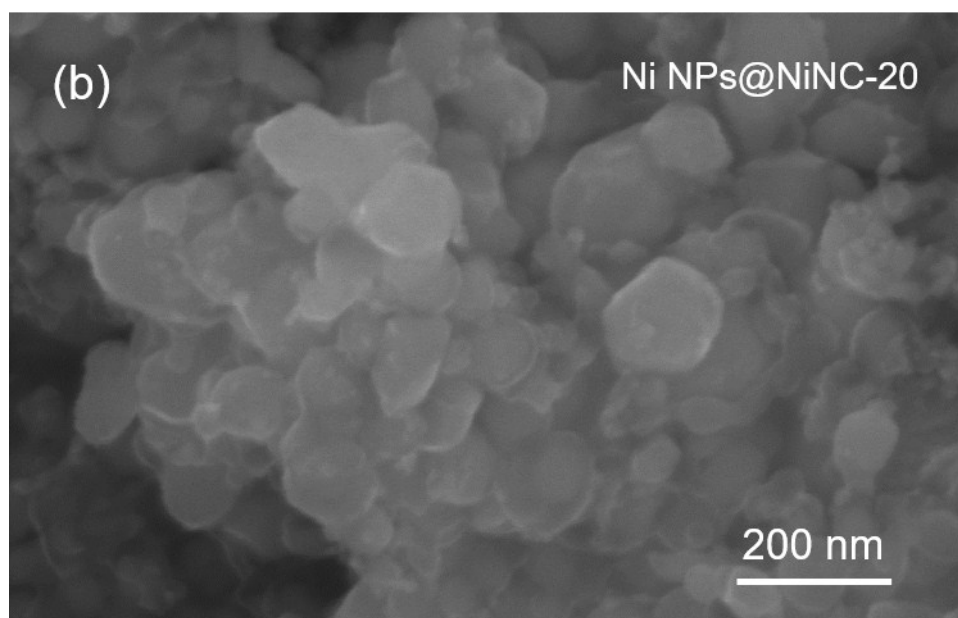
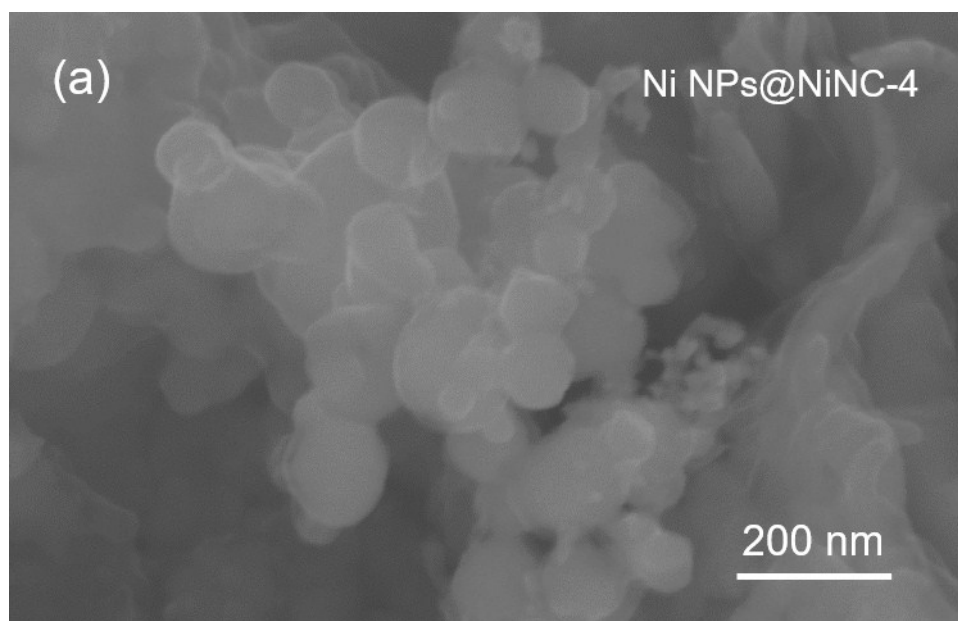


Fig. S3 SEM images for (a) Ni NPs@NiNC-4 and (b) Ni NPs@NiNC-20.

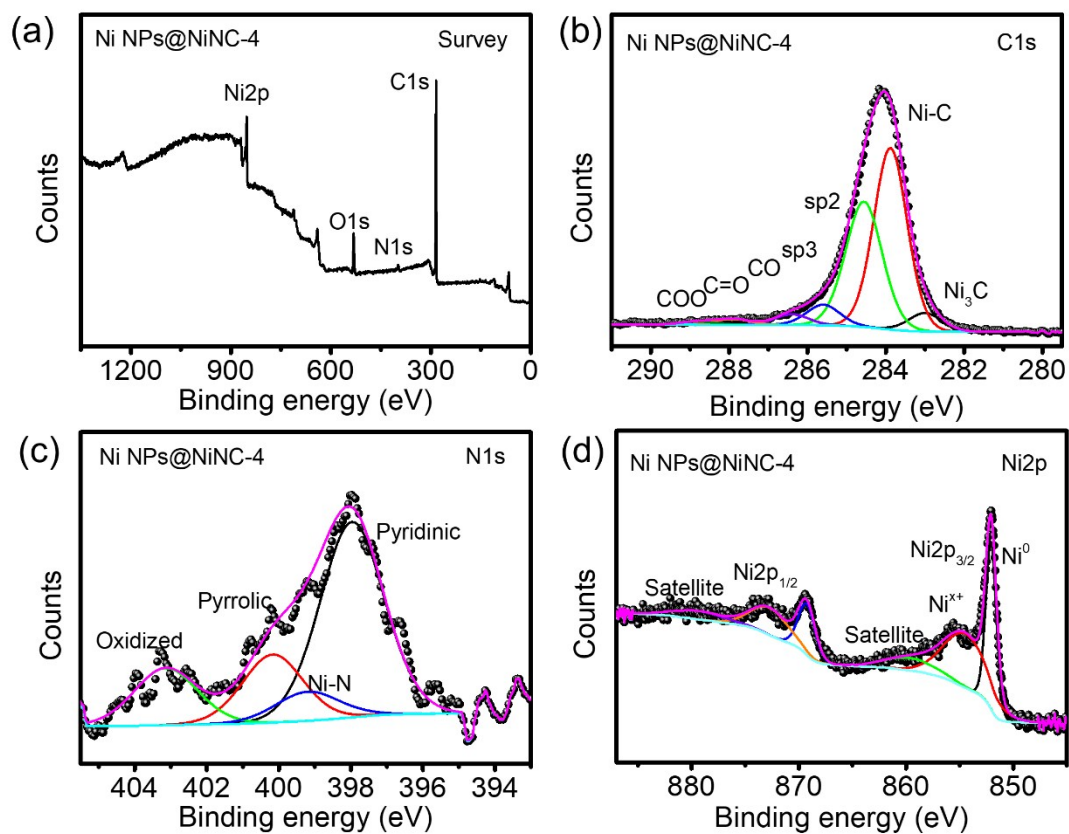


Fig. S4 XPS spectra of Ni NPs@NiNC-4. (a) Survey spectrum. (b-d) High resolution spectra of C_{1s}, N_{1s}, and Ni_{2p}.

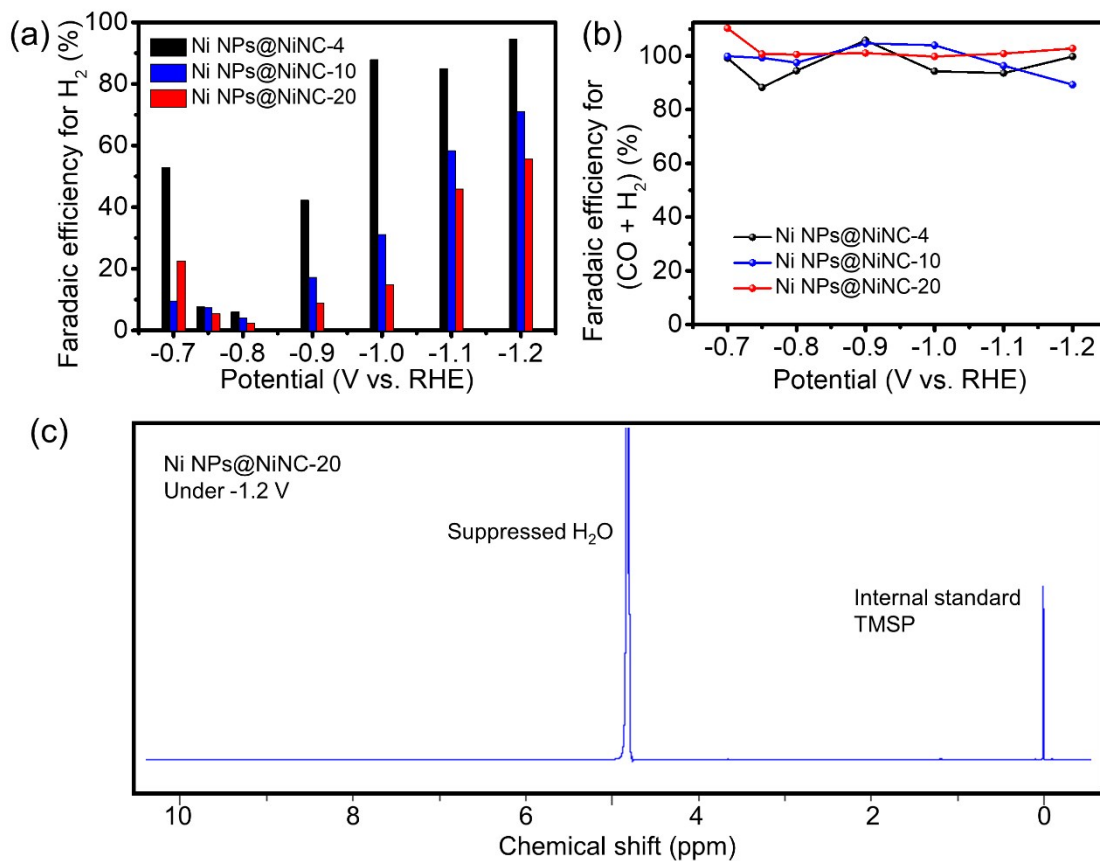


Fig. S5 (a) H₂ and (b) CO+H₂ Faradaic efficiencies of Ni NPs@NiNC-4, Ni NPs@NiNC-10, and Ni NPs@NiNC-20. (c) ¹H NMR spectrum of electrolyte electrolyzed under -1.2 V for 1 h on the Ni NPs@NiNC-20 catalysts. No detectable liquid products were produced during the electrolysis process.

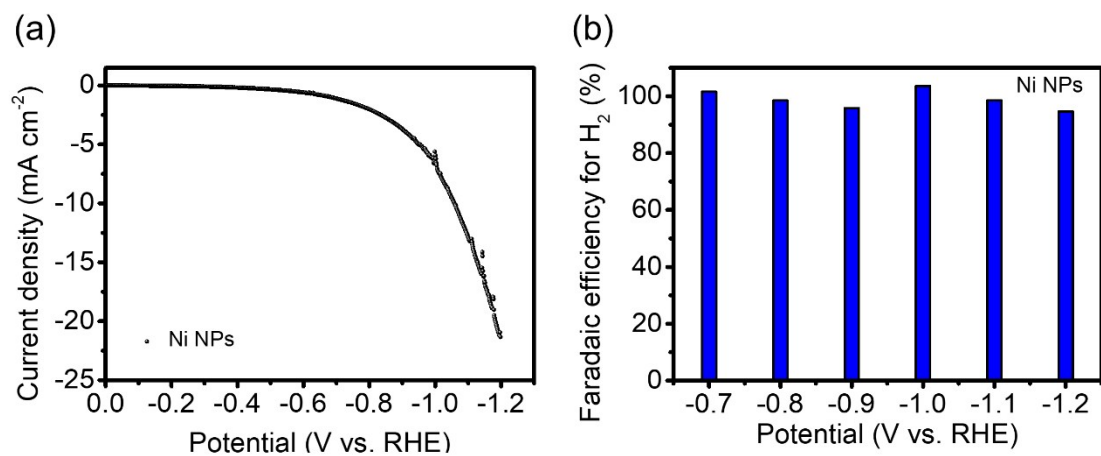


Fig. S6 (a) LSV plot with scan rate of 100 mV s⁻¹ and (b) Faradaic efficiencies for H₂ of the bared Ni NPs catalysts.

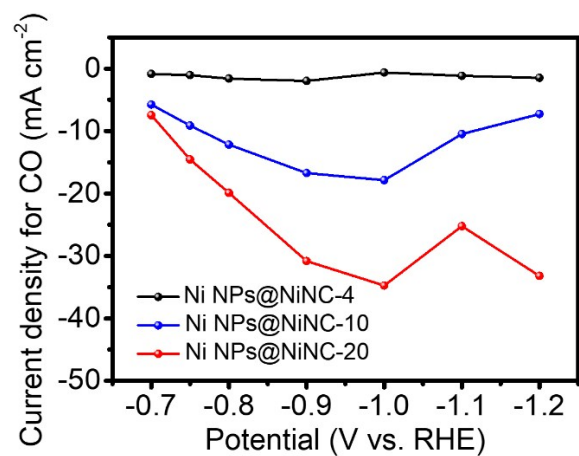


Fig. S7 CO formation current densities at specific potentials of Ni NPs@NiNC-4 (black), Ni NPs@NiNC-10 (blue), and Ni NPs@NiNC-20 (red).

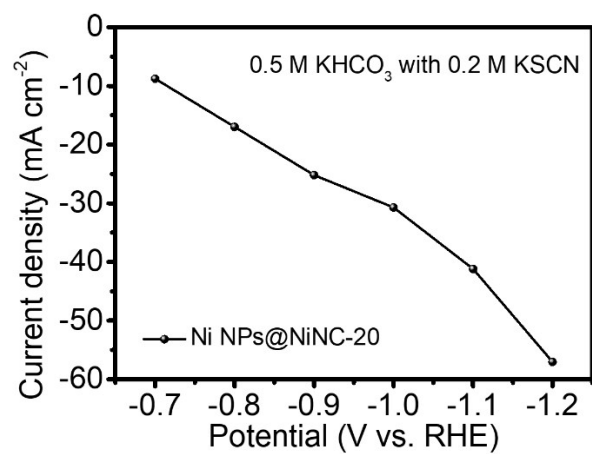


Fig. S8 Current densities of Ni NPs@NiNC-20 with existence of KSCN in KHCO₃ electrolyte at different applied potentials.

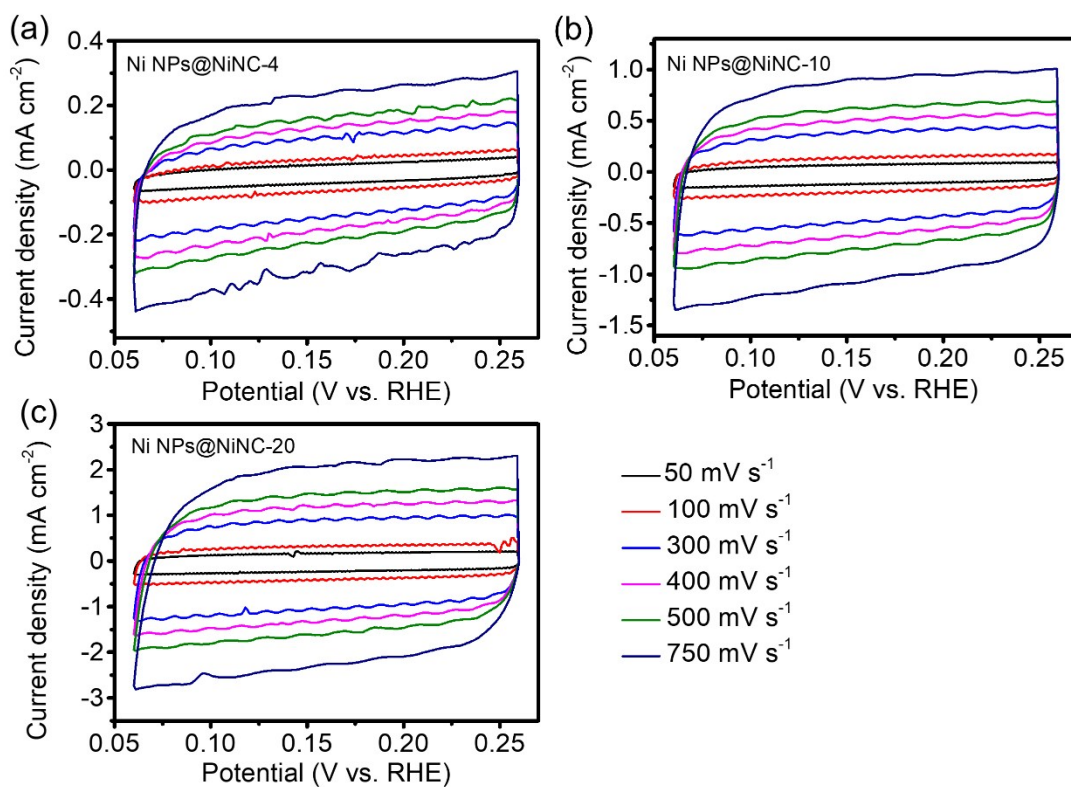


Fig. S9 Cyclic voltammetry plots implemented at different scan rates (50, 100, 300, 400, 500, and 750 mV s⁻¹) in a non-Faradaic region from +0.06 to +0.26 V in the CO₂-saturated 0.5 M KHCO₃.

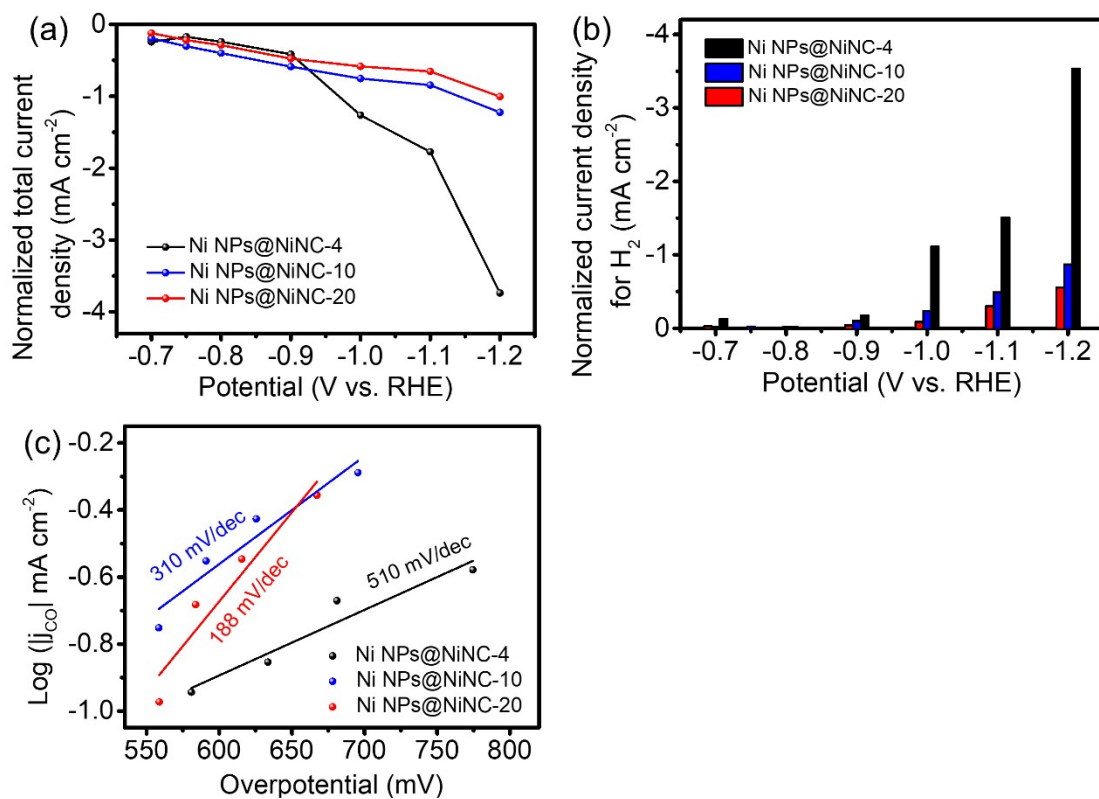


Fig. S10 ECSA normalized analysis of Ni NPs@NiNC-4 (black), Ni NPs@NiNC-10 (blue), and Ni NPs@NiNC-20 (red). (a) Total current densities. (b) Specific current densities for H₂. (c) Tafel plots based on the ECSA normalized current densities for CO generation.

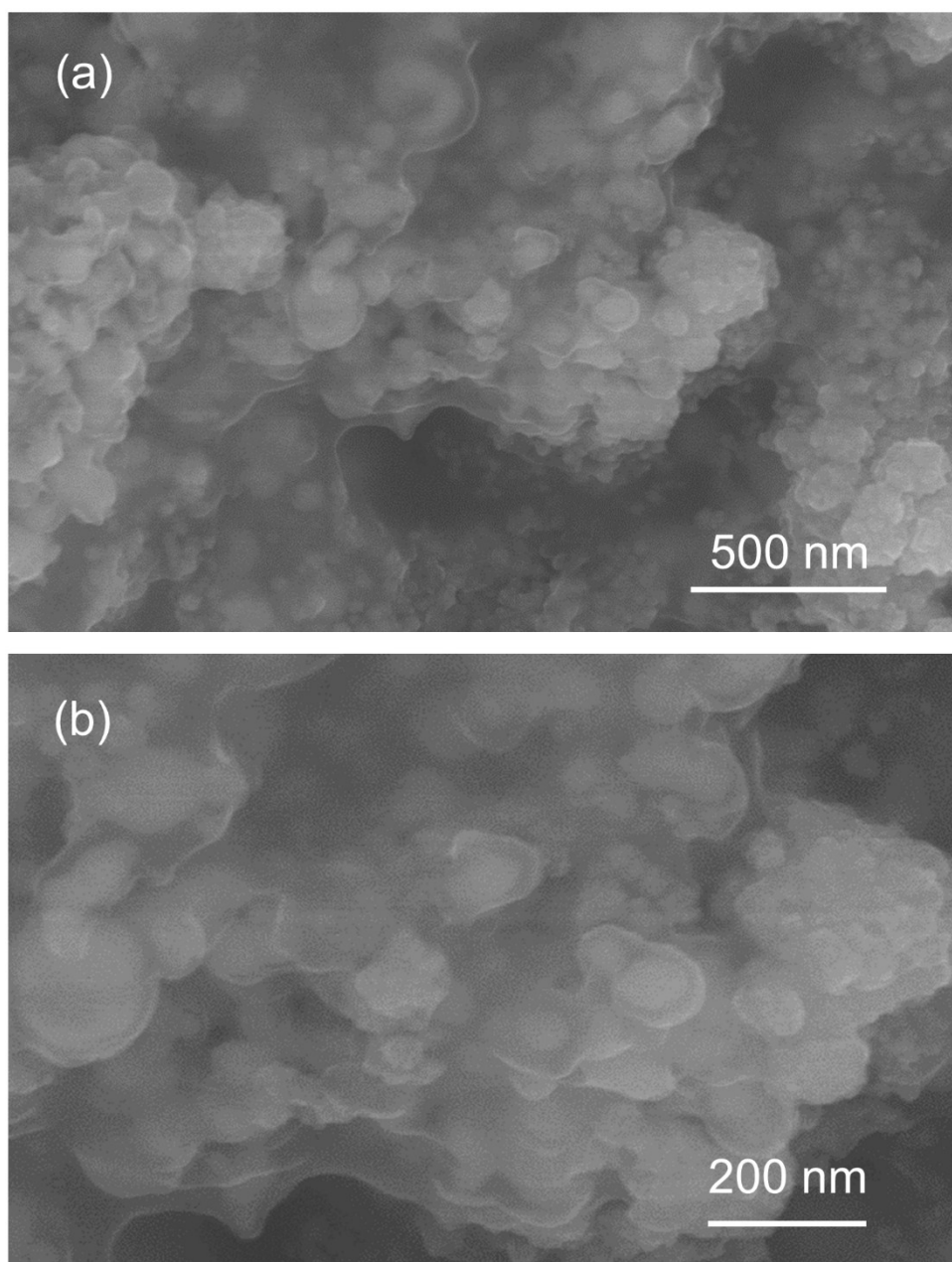


Fig. S11 SEM images of Ni NPs@NiNC-10 after 12 h electrolysis under -0.8V. The typical core-shell structure is remained.

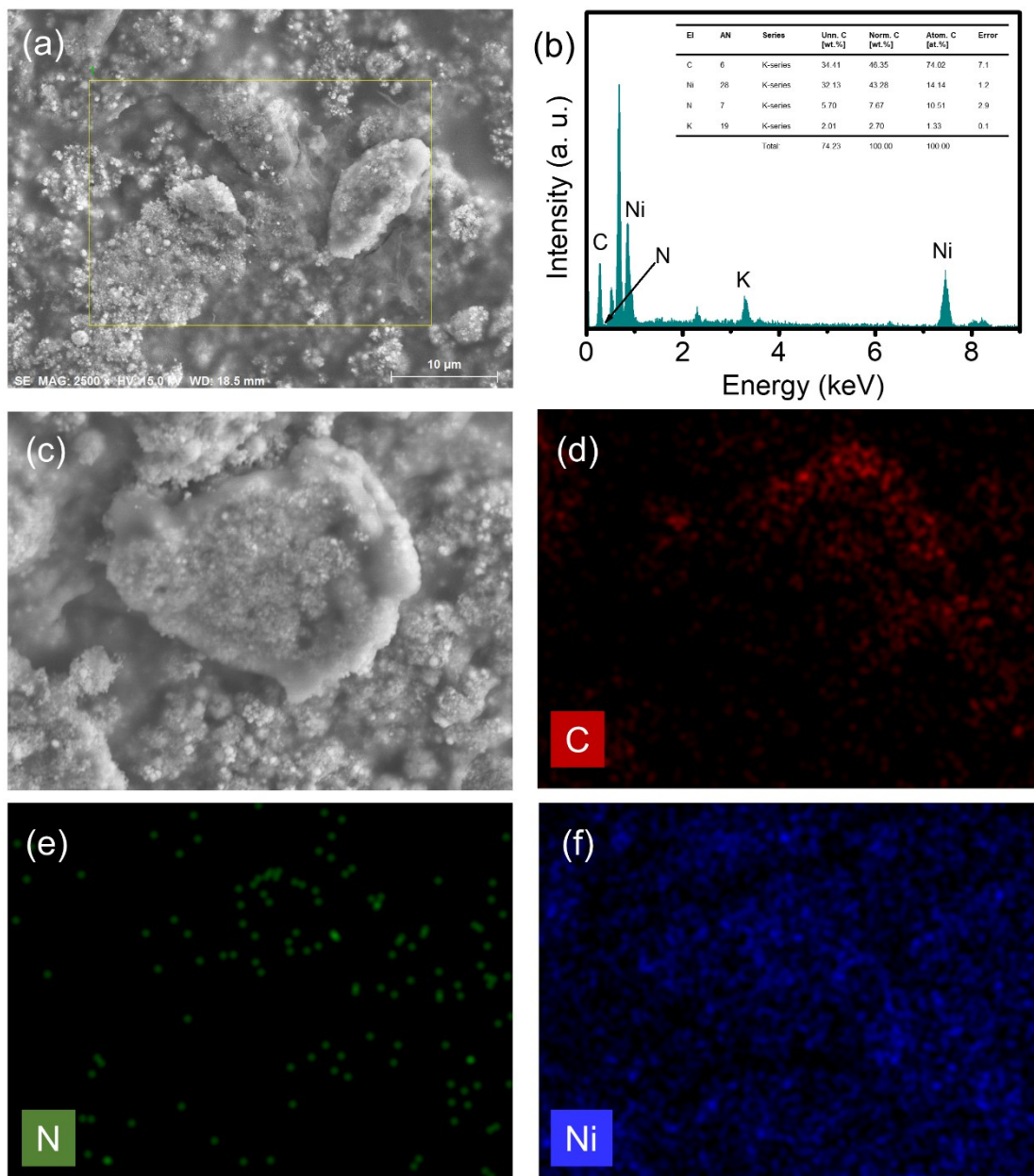


Fig. S12 Energy spectra analysis of Ni NPs@NiNC-10 after 12 h electrolysis under -0.8 V. (a, b) Selected region energy spectrum. (c-f) Elements mapping by surface sweep analysis.

Table S1 Elements analysis from XPS survey spectra for Ni NPs@NiNC-4 and Ni NPs@NiNC-10 by integral area.

Sample	C 1s		N 1s		O 1s		Ni 2p	
	BE (eV)	Area (%)						
Ni NPs@NiNC-4	285.6	45.3	398.0	2.9	531.0	13.2	852.1	38.6
Ni NPs@NiNC-10	285.6	33.1	398.0	8.0	531.0	12.5	852.1	46.4

Table S2 Ni element with different oxidation state analysis based on the high-resolution Ni 2p XPS spectra of Ni NPs@NiNC-4 and Ni NPs@NiNC-10.

Sample	Ni ⁰		Ni ^{x+}		Ni ^{x+} /Ni ⁰
	BE (eV)	Area (%)	BE (eV)	Area (%)	
Ni NPs@NiNC-4	852.1	25.0	854.0	33.3	1.3
Ni NPs@NiNC-10	852.1	16.4	854.0	35.9	2.2

Table S3 Summary of the performances of Ni-based catalysts for CO₂ reduction in aqueous solution.

Catalysts	Electrolyte	Product	FE (%)	E (V)	j (mA cm ⁻²)	Ref.
Ni NPs@NiNC	0.5 M KHCO₃	CO	98.3	-0.80	20.2	This work
Ni-N _x -C	0.1 M KHCO ₃	CO	~85	-0.75	~10	1
Ni-N ₄ -C	0.5 M KHCO ₃	CO	99	-0.81	28.6	2
Ni SAs/N-C	0.5 M KHCO ₃	CO	71.9	-1.00	10.48	3
Ni-N-RGO	0.5 M KHCO ₃	CO	97	-0.80	~23	4
Ni-N-C	0.5 M KHCO ₃	CO	93	-0.67	3.9	5
C-Zn ₁ Ni ₄ ZIF-8.	1 M KHCO ₃	CO	92	-1.03	~71.5	6
A-Ni-NSG	0.5 M KHCO ₃	CO	98	-0.72	22.4	7
SE-Ni SAs@PNC	0.5 M KHCO ₃	CO	~97	-0.8	~8	8
NiSA-N-CNTs	0.5 M KHCO ₃	CO	91.3	-0.7	~25.2	9
NiSA-H-CPs	0.5 M KHCO ₃	CO	97	-1.0	48.66	10
NiSA-N-CNT	0.5 M KHCO ₃	CO	91.3	-0.7	25.7	11
Ni SAs/NCNTs,	0.5 M KHCO ₃	CO	95	-1.0	57.1	12
Ni/N-C	0.5 M KHCO ₃	CO	97.1	-0.61	~20	13
Ni-NC SAC	0.5 M KHCO ₃	CO	89	-0.85	33.7	14
Ni-NCB	0.5 M KHCO ₃	CO	99	-0.68	~10	15
CoNi-NC	0.5 M KHCO ₃	CO	~50	-0.9	51	16
Ni@NCNTs	0.5 M KHCO ₃	CO	99.1	-0.8	8.01	17
Ni ₃ N/MCNT	0.5 M NaHCO ₃	CO	89	-0.73	6.5	18
Ni ₃ N/C	0.5 M NaCl	CO	85.7	-0.9	7.35	19

Supporting references:

1. W. Ju, A. Bagger, G.-P. Hao, A. S. Varela, I. Sinev, V. Bon, B. Roldan Cuenya, S. Kaskel, J. Rossmeisl and P. Strasser, *Nat. Commun.*, 2017, **8**, 944.
2. X. Li, W. Bi, M. Chen, Y. Sun, H. Ju, W. Yan, J. Zhu, X. Wu, W. Chu, C. Wu and Y. Xie, *J. Am. Chem. Soc.*, 2017, **139**, 14889-14892.
3. C. Zhao, X. Dai, T. Yao, W. Chen, X. Wang, J. Wang, J. Yang, S. Wei, Y. Wu and Y. Li, *J. Am. Chem. Soc.*, 2017, **139**, 8078-8081.
4. H.-Y. Jeong, M. Balamurugan, V. S. K. Choutipalli, J. Jo, H. Baik, V. Subramanian, M. Kim, U. Sim and K. T. Nam, *Chem. – A Eur. J.*, 2018, **24**, 18444-18454.
5. X.-M. Hu, H. H. Hval, E. T. Bjerglund, K. J. Dalgaard, M. R. Madsen, M.-M. Pohl, E. Welter, P. Lamagni, K. B. Buhl, M. Bremholm, M. Beller, S. U. Pedersen, T. Skrydstrup and K. Daasbjerg, *ACS Catal.*, 2018, **8**, 6255-6264.
6. C. Yan, H. Li, Y. Ye, H. Wu, F. Cai, R. Si, J. Xiao, S. Miao, S. Xie, F. Yang, Y. Li, G. Wang and X. Bao, *Energy Environ. Sci.*, 2018, **11**, 1204-1210.
7. H. B. Yang, S.-F. Hung, S. Liu, K. Yuan, S. Miao, L. Zhang, X. Huang, H.-Y. Wang, W. Cai, R. Chen, J. Gao, X. Yang, W. Chen, Y. Huang, H. M. Chen, C. M. Li, T. Zhang and B. Liu, *Nat. Energy*, 2018, **3**, 140-147.
8. J. Yang, Z. Qiu, C. Zhao, W. Wei, W. Chen, Z. Li, Y. Qu, J. Dong, J. Luo, Z. Li and Y. Wu, *Angew. Chem. Int. Ed.*, 2018, **57**, 14095-14100.
9. C. Yi, Z. Shiyong, J. Bernt, V. Jean-Pierre, S. Martin, R. M. R., C. Min, L. Chang, C. M. F., M. Roland, C. Hui-Ming, Y. Shi-Ze and J. S. Ping, *Adv.*

- Mater.*, 2018, **30**, 1706287.
10. C. Zhao, Y. Wang, Z. Li, W. Chen, Q. Xu, D. He, D. Xi, Q. Zhang, T. Yuan, Y. Qu, J. Yang, F. Zhou, Z. Yang, X. Wang, J. Wang, J. Luo, Y. Li, H. Duan, Y. Wu and Y. Li, *Joule*, 2018, **3**, 584-594.
 11. S. Zhao, Y. Cheng, J.-P. Veder, B. Johannessen, M. Saunders, L. Zhang, C. Liu, M. F. Chisholm, R. De Marco, J. Liu, S.-Z. Yang and S. P. Jiang, *ACS Appl. Energy Mater.*, 2018, **1**, 5286-5297.
 12. P. Lu, Y. Yang, J. Yao, M. Wang, S. Dipazir, M. Yuan, J. Zhang, X. Wang, Z. Xie and G. Zhang, *Appl. Catal. B: Environ.*, 2019, **241**, 113-119.
 13. D. Tan, C. Cui, J. Shi, Z. Luo, B. Zhang, X. Tan, B. Han, L. Zheng, J. Zhang and J. Zhang, *Nano Research*, 2019, **12**, 1167-1172.
 14. L. Zhao, Y. Zhang, L.-B. Huang, X.-Z. Liu, Q.-H. Zhang, C. He, Z.-Y. Wu, L.-J. Zhang, J. Wu, W. Yang, L. Gu, J.-S. Hu and L.-J. Wan, *Nat. Commun.*, 2019, **10**, 1278.
 15. T. Zheng, K. Jiang, N. Ta, Y. Hu, J. Zeng, J. Liu and H. Wang, *Joule*, 2019, **3**, 265-278.
 16. Q. He, D. Liu, J. H. Lee, Y. Liu, Z. Xie, S. Hwang, S. Kattel, L. Song and J. G. Chen, *Angew. Chem. Int. Ed.*, 2020, **59**, 3033-3037.
 17. W. Zheng, C. Guo, J. Yang, F. He, B. Yang, Z. Li, L. Lei, J. Xiao, G. Wu and Y. Hou, *Carbon*, 2019, **150**, 52-59.
 18. Z. Wang, P. Hou, Y. Wang, X. Xiang and P. Kang, *ACS Sustain. Chem. Eng.*, 2019, **7**, 6106-6112.

19. P. Hou, X. Wang, Z. Wang and P. Kang, *ACS Appl. Mater. Interfaces*, 2018, **10**, 38024-38031.